Journal of Power Sources 209 (2012) 65–71

Contents lists available at SciVerse ScienceDirect

Journal of Power Sources

journal homepage: www.elsevier.com/locate/jpowsour

Three-dimensional simulation to study the influence of foil thickness on residual stress in the bonded compliant seal design of planar solid oxide fuel cell

Wen-chun Jiang[a,b,c,*], Yu-cai Zhang[b], Wanchuck Woo[c], S.T. Tu[a]

[a] Key Laboratory of Pressure System and Safety (MOE), School of Mechanical and Power Engineering, East China University of Science and Technology, Shanghai 200237, PR China
[b] College of Chemical Engineering, China University of Petroleum, Qingdao 266555, PR China
[c] Neutron Science Division, Korea Atomic Energy Research Institute, Daejeon 305-353, South Korea

ARTICLE INFO

Article history:
Received 31 January 2012
Accepted 16 February 2012
Available online 25 February 2012

Keywords:
Solid oxide fuel cell
Bonded compliant seal
Foil thickness
Residual stress

ABSTRACT

Bonded compliant seal (BCS) design, which uses a thin S-shaped foil to connect the cell and frame by brazing, is a new sealing method for planar solid oxide fuel cell (SOFC). This paper studies the brazed residual stress in BCS design of a planar SOFC by three-dimensional finite element method. The effect of foil thickness on residual stress has been investigated. The results show that the peak residual stresses are located in S-shaped foil and BNi2 filler metal and have exceeded the yield strength. Therefore S-shaped foil and BNi2 filler metal are the most dangerous zone. The foil thickness has a great effect on residual stress. The peak residual stresses in foil and BNi2 are increased with the foil thickness increase. With the foil thickness increase, the residual stresses in window frame are increased, while residual stresses in Ag–CuO filler metal are decreased.

1. Introduction

Planar solid oxide fuel cell (SOFC), which converts the chemical energy into electrical power by electrochemical reaction, is one of the most attractive candidates for the next generation of power sources [1–3]. Planar SOFC operates at high temperature and oxidizing atmosphere, which can easily lead to leakage. Therefore the most key is the sealing technology for planar SOFC [4–9]. So far, three main methods including the rigid-bonded seal [10–12], compressive seal [13–15] and the bonded compliant seal (BCS) [16,17] have been used to seal the planar SOFC stack.

For rigid-bonded seal, the metals such as silver or gold can be used as the sealing materials to combine the SOFC components [18–20]. Silver and gold are stable at air but the disadvantage is that they are expensive and increase the manufacturing cost. Therefore, glass or glass–ceramic materials are commonly used in the rigid-bonded seal [21–23]. Due to the mismatch of thermal expansion coefficient (CTE) between the SOFC components, thermal stresses are generated inevitably and have a great effect on cracks. The repeated thermal cycling during the long-term operation may lead to the crack and leakage since the glass–ceramic is brittle [24].

For compressive seal, a pressure must be applied to achieve the tightness [25]. In this design, the generated thermal stress is lower because it does not rigidly bond the SOFC components and allows some deformation. Silver and Mica are used as gasket and base materials respectively, but which increases the leak rate [26–28]. It was also found that the silver with 7.5% copper was too strong to deform with the applied pressure, leading to poor tightness. Compared with the rigid-bonded seal, compressive seal has poorer tightness or unfavorable reaction, leading to a lower cell performance. Therefore compressive seal is also not suitable for a long-term operation [29,7,30].

The bonded compliant seal (BCS), which is designed by Weil et al. [16], combines the advantages of rigid-bonded method and compressive seal method. It uses a thin deformable foil metal to braze the adjacent metal and ceramic components, through which the different extents of the deformation between the adjacent components are accommodated. Therefore it not only has good tightness, but also can absorb some thermal deformation by the sealing foil to reduce the thermal stress. It has been proved that the BCS structure presents good strength in as-brazed and thermally cycled conditions [16]. Residual stress is one of the reasons that cause leakage and failure in BCS structure, which has attracted more attention in recent years [31–35]. Weil and Koeppel [36] found that the BCS design offered obvious advantages over glass–ceramic sealing method based on thermal stress analysis. Jiang and Chen [31] also performed thermal stress analysis to an operating planar SOFC with BCS design by finite element method (FEM), and the effects of temperature non-uniformity and cell voltage on thermal stress

* Corresponding author at: Key Laboratory of Pressure System and Safety (MOE), School of Mechanical and Power Engineering, East China University of Science and Technology, Shanghai 200237, PR China. Tel.: +86 2164253425; fax: +86 2164253425.
E-mail address: jiangwenchun@126.com (W.-c. Jiang).

0378-7753/$ – see front matter © 2012 Elsevier B.V. All rights reserved.
doi:10.1016/j.jpowsour.2012.02.060

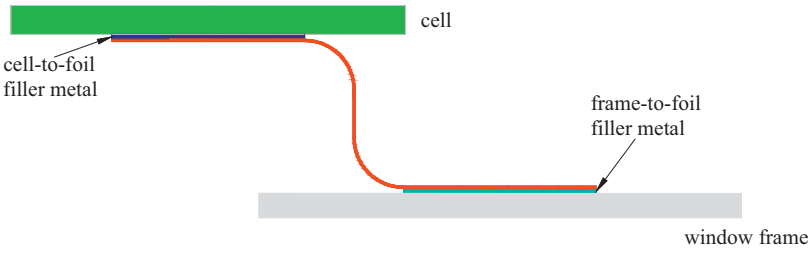

Fig. 1. The cross section of the BCS structure.

Table 1
Dimensions and materials for the components of BCS structure [36].

Component	Cell	Cell-to-foil braze	Foil	Foil-to-frame braze	Frame
Thickness (μm)	600	100	20	100	500
Material	Ni–YSZ/YSZ	Ag–4 mol% CuO	FeCrAlY	BNi-2	Haynes 214

were discussed. We [37] performed a preliminary analysis of brazed residual stress in BCS design by a two-dimensional finite element method (FEM), which provides some reference for design; but the window frame are constrained rigidly, which may lead to an overestimation of residual stresses and the out-of-plane principal stress was also not analyzed. In addition, the thickness design of foil metal plays an important role on the performance of SOFC. Therefore here we use three-dimensional FEM to study the foil thickness on brazed residual stress.

2. Modeling

2.1. Finite element model

Fig. 1 shows the cross section of the BCS structure. An S-shaped sealing foil is brazed to the cell and window frame by silver-based filler metal (Ag–4%CuO) and BNi2 filler metal, respectively. The thickness of each component is listed in Table 1 [36]. The residual stress distributions were analyzed by a commercial FE code ABAQUS. Due to the cell geometry is 4-fold symmetric, only one-quarter model was built to decrease the computation time. A three-dimensional (3D) finite element model is built, as presented in Fig. 2. The finite element meshing is shown in Fig. 3. There are total 66 798 elements and 90 297 nodes in the 3D model.

2.2. Brazing

The planar SOFC stacking is brazed in the vacuum furnace. At first the stacking is heated to 600 °C at 10 °C min^{-1} and the temperature is held for about 40 min to volatilize the binder. Then it is heated to the brazing temperature of 1050 °C and held about 25 min. At last, the assembly is cooled to the ambient temperature in the furnace.

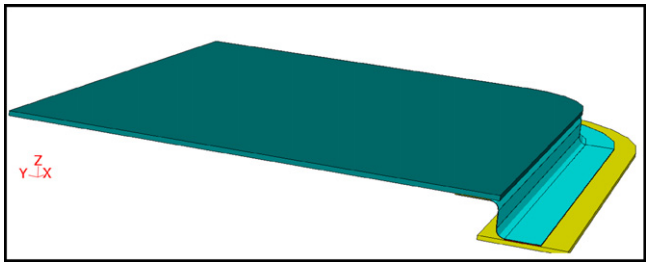

Fig. 2. Finite element model.

2.3. Simulation procedure

At high temperature, the assembly is at zero stress state. Therefore the residual stress is simulated during the cooling from brazing temperature (1050 °C) to 20 °C. For the present used materials, solid-state phase transformation does not occur. Therefore, the total strain rate can be decomposed into elastic strain, plastic strain and thermal strain, respectively. Elastic strain is modeled using the isotropic Hooke's law with temperature-dependent Young's modulus and Poisson's ratio. The thermal strain is calculated using the temperature-dependent CTE. For plastic strain, a rate-independent plastic model is employed with Von Mises yield surface, temperature-dependent mechanical properties and linear kinematic hardening model. In kinematic hardening model, the yield strength surface does not change its shape, size or orientation, but rather its center as the yield surface translates in stress space, as shown in Fig. 4. The kinematic model is commonly used in FE analyses of residual stress.

2.4. Material properties

The materials of the components in BCS structure are listed in Table 1. Temperature-dependent properties of materials are incorporated. The material properties relevant to thermal stress are

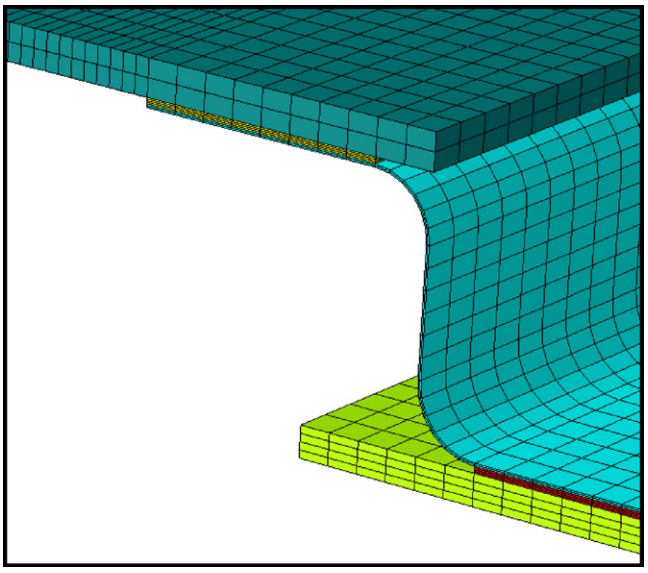

Fig. 3. Finite element meshing.

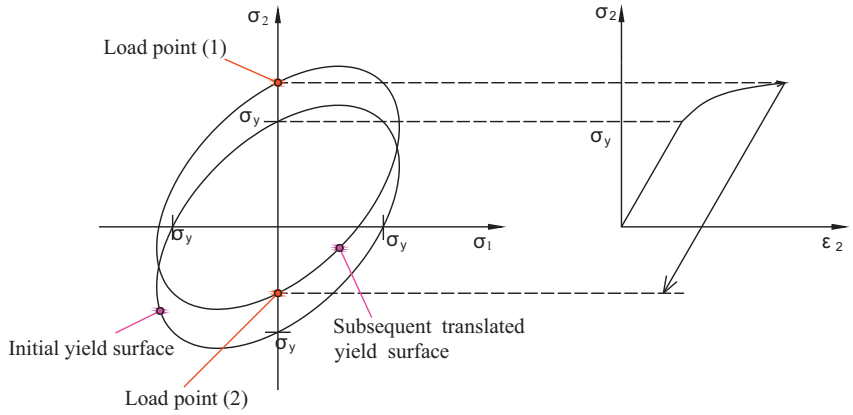

Fig. 4. Kinematic hardening model.

elastic modulus, yield stress, Poisson's ratio, and the coefficient of thermal expansion (CTE). In fact, the cell in the planar stacks is a composite structure composed of anode, electrolyte layer and cathode layer. However in the present study, the attention is focused on the joint of sealing foil-to-window frame, and therefore the material of the cell is assumed to be the same as anode material (Ni-YSZ). The material properties are listed in Table 2.

2.5. Boundary and constrained conditions

The symmetric boundary conditions were applied in the two cross sections. And all the nodes on the bottom face of the window frame were constrained in *z*-direction. Thus the rigid body motion was avoided.

Table 2
Material properties.

Materials	Properties: E is Young's modulus (GPa); α is coefficient of thermal expansion ($^\circ C^{-1} \times 10^{-6}$); σ_s yield strength (MPa); μ is Poisson's ratio
Haynes 214	E: 220 (20 °C), 210 (100 °C), 204 (200 °C), 177 (400 °C), 184 (600 °C), 162 (800 °C); α: 13.3 (200 °C), 14.1 (400 °C), 15.2 (600 °C), 16.6 (800 °C); σ_s: 620 (25 °C), 570 (540 °C), 540 (650 °C),320 (870 °C), 65 (1000 °C); μ: 0.28
FeCrAlY	E: 220 (20 °C), 210 (100 °C), 205 (200 °C), 190 (400 °C), 170 (600 °C), 150 (800 °C); α: 11.0 (250 °C), 12.0 (500 °C), 14.0 (750 °C), 15.0 (1000 °C); σ_s: 310 (25 °C), 170 (427 °C), 120 (593 °C),80 (650 °C), 70 (705 °C), 35 (800 °C); μ: 0.28
BNi2	E: 205 (20 °C), 200 (100 °C), 195 (200 °C), 184 (400 °C), 172 (600 °C), 161 (800 °C); α: 13.4 (25 °C), 15.0 (200 °C), 16.8 (400 °C), 18.2 (600 °C), 19.9 (800 °C); σ_s: 300 (25 °C), 220 (400 °C), 180 (700 °C), 160 (800 °C), 90 (1000 °C); μ: 0.28
Ag–CuO	E: 52 (25 °C), 49.6 (185 °C), 49.6 (300 °C); α: 15 (25 °C), 15.0 (200 °C), 15.0 (400 °C), 15.0 (600 °C), 15.0 (800 °C); σ_s: 335 (25 °C), 235 (185 °C), 100 (280 °C), 85 (373 °C), 20 (800 °C); μ: 0.38
Cell	E: 120 (25 °C), 116 (100 °C), 1.0 (200 °C), 97 (400 °C), 78 (800 °C); α: 12 (25 °C), 12.0 (800 °C); μ: 0.32

3. Results and discussion

Residual stress components from FE analysis are obtained in the following direction: (1) transverse stress S11, represents the stress in *X*-axis direction; (1) longitudinal stress S22, represents the stress in *Y*-axis direction; (2) Thickness stress S33, refers the stress in *Z*-axis direction. In this paper due to the geometry model has 4-fold symmetry, therefore S11 in the *x*-direction is the same as S22 in the *y*-direction, and S11 in the *y*-direction is the same as S22 in the *x*-direction.

3.1. Residual stress distribution

Fig. 5 shows the contours of transverse stress in cell, Ag–CuO filler metal, foil, BNi2 and window frame. In cell as shown in Fig. 5(a), the peak S11 is 45 MPa and the stress is relatively small, and the residual stress is concentrated on the edge and then decreases to the center. In Ag–CuO filler metal, the peak S11 is about 174 MPa which is shown in the half part, and S11 in the other half part is about 137 MPa, as shown in Fig. 5(b). In S-shaped foil, S11 is non-uniform. The peak stress is 286 MPa, which is shown in the part connected to Ag–CuO filler metal. In the part that connected to the BNi2, S11 shows a compressive stress of 324 MPa, as shown in Fig. 5(c). In filler metal BNi2, the peak stress is 332 MPa as presented on the edge of filler metal as shown in Fig. 5(d). S11 in the window frame is also small and its peak is about 42 MPa, as shown in Fig. 5(e).

Fig. 6 shows the contours of thickness stress in BCS components. It is shown that the maximum stress, 208 MPa, is shown in the foil. While the thickness stress in cell, Ag–CuO filler metal, BNi2 and window frame are very small and their peaks are 21, 13, 17 and 16 MPa, respectively. This phenomenon proves that the S-shaped foil can deform plastically and elastically along the vertical crease between the upper and lower sealing surfaces. S-shaped foil plays a role like a spring, and some stresses in BCS structure can be absorbed in the foil as elastic and plastic deformation. Therefore the residual stresses in other components are very small, which can decrease the leakage risk.

3.2. Effect of foil thickness

In BCS design, the foil thickness plays an important role on reducing the stresses in the structure, which is discussed here. Keeping the rest parameters constant, the foil thickness is changed to discuss its effect. S33 is very small and is not considered in the following discussion.

The maximum residual stresses in cell, Ag–CuO, foil, BNi2 and window frame with different foil thickness are listed in Table 3.

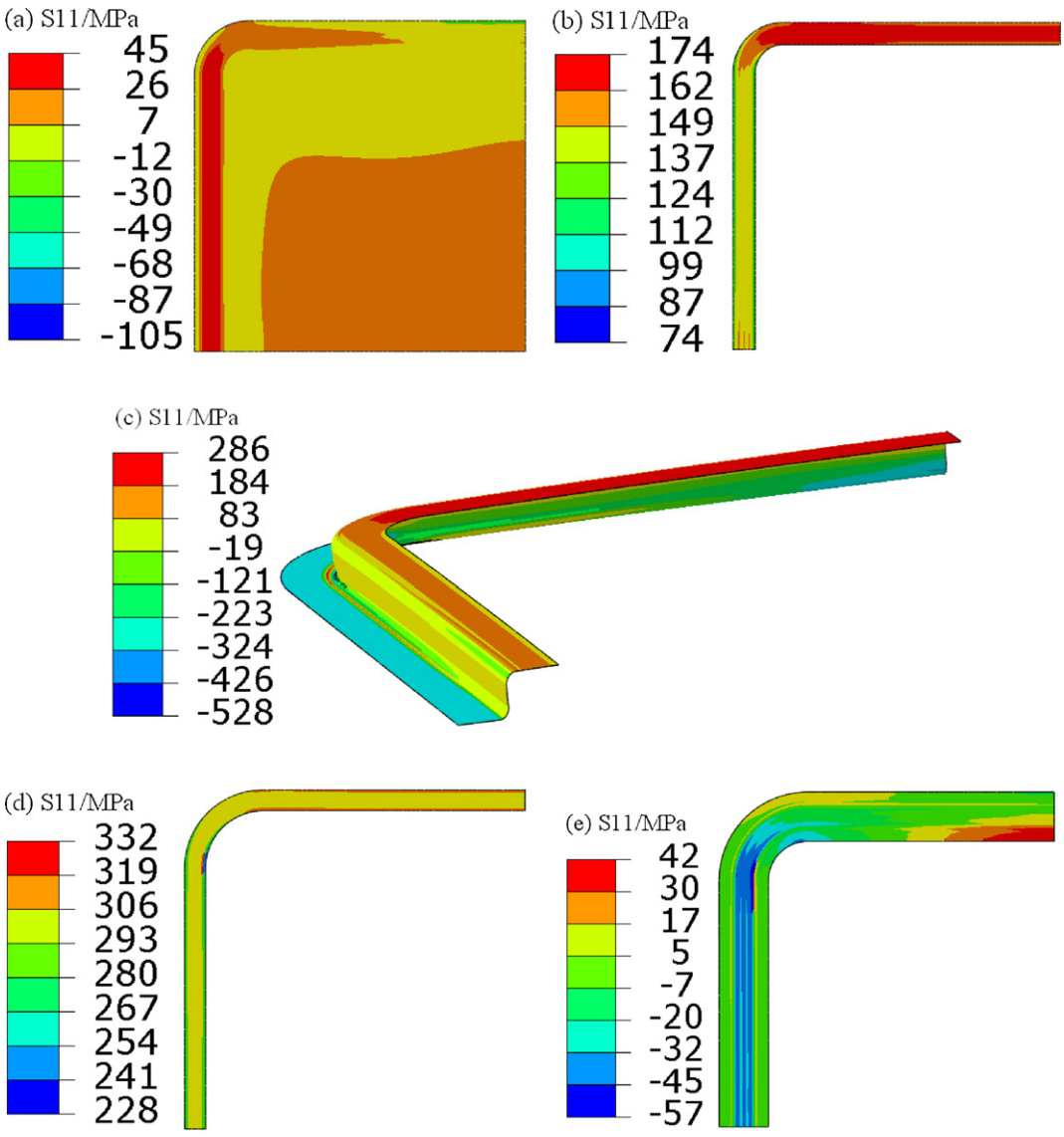

Fig. 5. S11 contours in cell (a), Ag–CuO (b), foil (c), (d) BNi2 and window frame (e).

It is shown that the maximum residual stresses in cell, foil, BNi2 and window frame are increased as the foil thickness increase. But the foil thickness has little influence on the peak residual stress in Ag–CuO. In order to investigate the effect of foil thickness on residual stress in each component, 4 reference paths as positioned in Figs. 7–10 are taken to analyze respectively.

Fig. 7 shows the effect of foil thickness on residual stress along path P1 in the window frame. It is shown that the residual stresses are increased as the foil thickness increases. When the foil thickness is below 50 μm, the residual stress along the 70% length is compressive. But when the foil thickness is 80 μm, almost 100% is tensile stress, and the peak S11 is also increased to 180 MPa as listed in Table 3. This means that the residual stress in the window frame is increased with the foil thickness increase, and especially it has a sudden increase when the foil thickness is 80 μm, and the peak stress is increased to 318 MPa as the foil thickness is 120 μm.

Fig. 8 shows the effect of foil thickness on residual stress along path P2 in BNi2. It is presented that the residual stress has reached the yield strength of BNi2, and the residual stresses along P2 are slightly increased as the foil thickness increases. The peak residual

Table 3
The maximum residual stresses in BCS structure with different foil thickness.

Max. stress	Thickness (μm)	Cell (MPa)	Ag–CuO (MPa)	Foil (MPa)	BNi2 (MPa)	Frame (MPa)
S11	20	45	174	286	332	42
	50	53	176	303	363	75
	80	67	171	359	358	180
	120	77	169	371	380	318
S33	20	21	13	208	17	16
	50	27	22	336	52	12
	80	30	15	345	50	24
	120	29	18	355	84	48

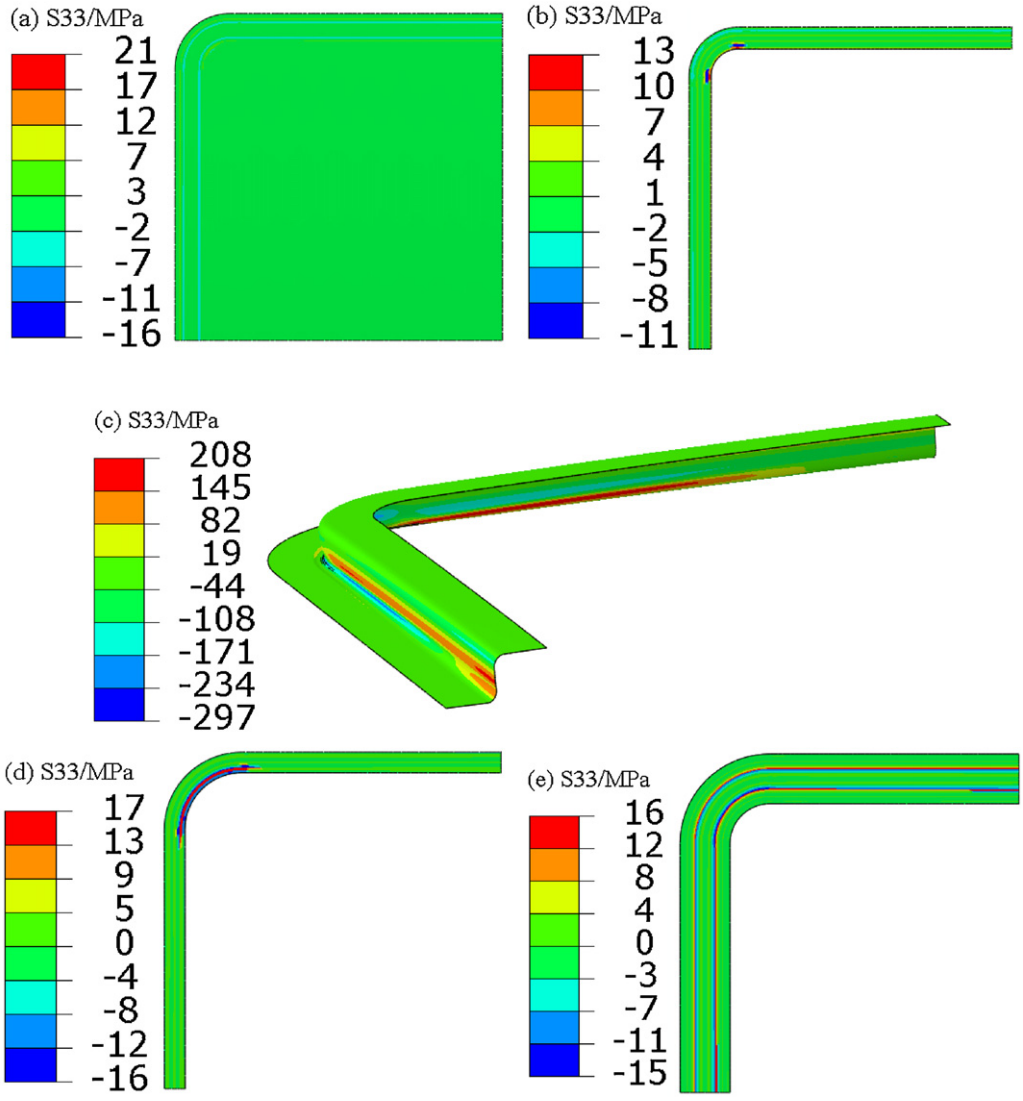

Fig. 6. S33 contours in cell (a), Ag–CuO (b), foil (c), (d) BNi2 and window frame (e).

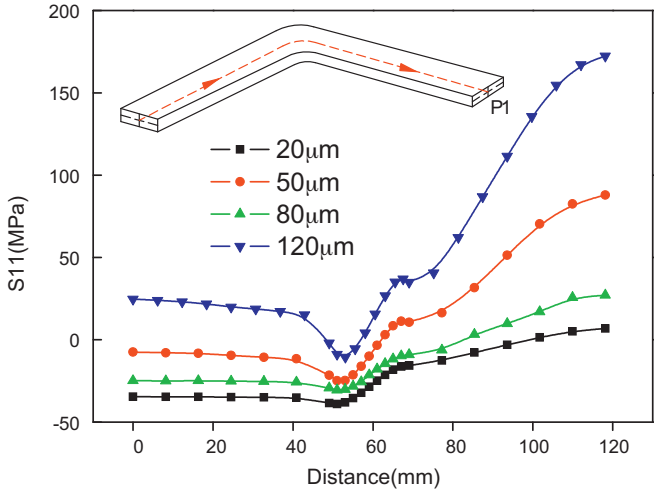

Fig. 7. Effect of foil thickness on residual stress in window frame.

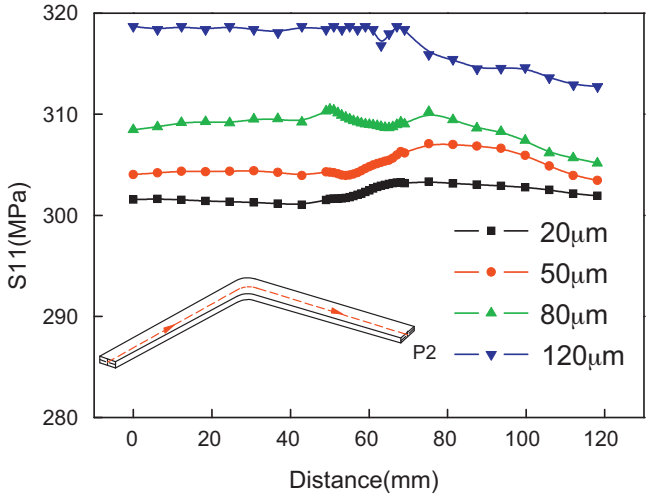

Fig. 8. Effect of foil thickness on residual stress in BNi2.

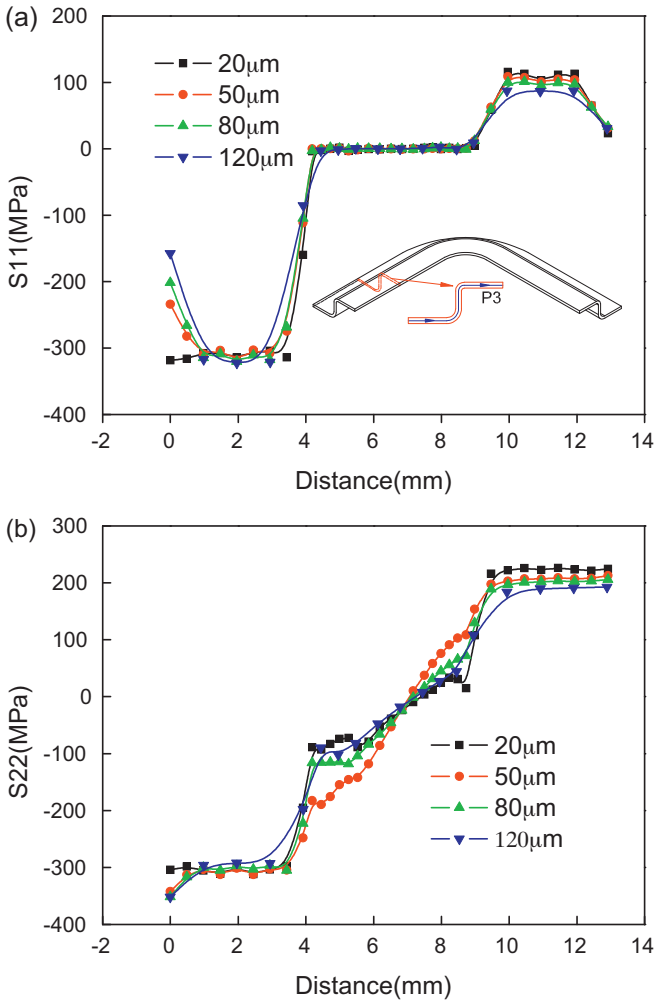

Fig. 9. Effect of foil thickness on residual stress in foil.

stresses are also increased, as listed in Table 3. As the foil thickness is 120 μm, the peak of S11 has increased to 380 MPa, which means that too thick foil can lead to large peak stress.

Fig. 9 shows the effect of foil thickness on residual stress along path P3 in the foil. Because the foil section does not have the 4-fold symmetry present in the other sections, therefore S11 and S22 are different as is shown. It is presented that the foil thickness has little effect on S11 and S22 along P3. But the foil thickness has greatly affected the peak stresses as listed in Table 3. When the foil thickness is increased to 80 μm, the peaks of S11 and S33 are increased to 359 MPa and 345 MPa, respectively, which has exceeded the yield strength about 35–40 MPa.

Fig. 10 shows the effect of foil thickness on residual stress along path P4 in Ag–CuO filler metal. With the foil thickness increase, the residual stresses are decreased. When the foil thickness is increased from 20 to 80 μm, about 20 MPa stress is decreased. This is because at the case of thinner filler metal thickness, the deformation gradient is very large, which brings more difficulty in stress relief and causes the large stress. Therefore, increasing the filler metal thickness can decrease the residual stress.

3.3. Discussion

As described above, large residual stresses are found, which would have a great effect on crack. Therefore the thickness design of the foil plays an important role on decreasing the residual stress. As the foil thickness increases, the residual stresses in the window frame are increased while residual stresses in Ag–CuO are decreased.

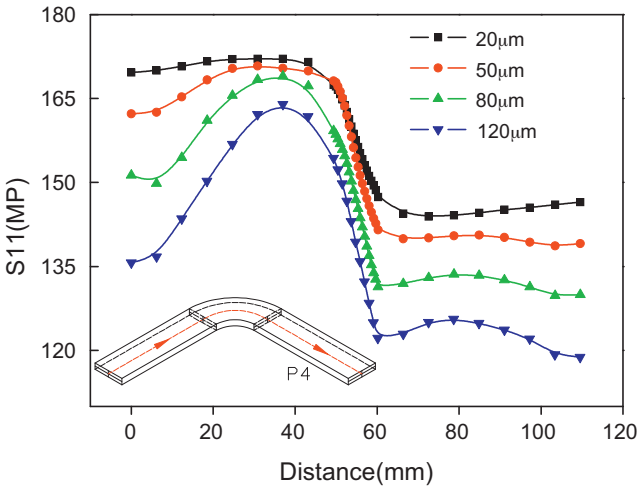

Fig. 10. Effect of foil thickness on residual stress in Ag–CuO.

As shown in Table 3 and Figs. 5–6, it is found that the biggest residual stresses are shown in the foil and BNi2. It means that the dangerous position has been changed from the cell to the foil itself, which improves the benefits of BCS design. Therefore, it is very necessary to pay special attention to the foil, and it is also very vital to determine a good design of foil thickness to ensure the strength requirement and safety. In the S-shaped foil, the foil thickness affects the peak stresses greatly. With the foil thickness increase, the peak stresses are found to increase. As the foil thickness increases to 80 μm, the peak residual stresses have exceeded its yield strength. As the foil thickness is further increased to 120 μm, the peak residual stress in BNi2 has been increased to 380 MPa and exceeded yield strength 80 MPa, meanwhile peak S11 in window frame has been suddenly increased to 318 MPa. In BNi2 filler metal, some brittle phases are generated after the brazing [38], therefore, the increased residual stresses can generate cracks and give threaten to the safety. As shown in Fig. 7, half of the stresses along P1 in window frame are compressive when the foil thickness is below 80 μm, but as the foil thickness increases to 120 μm all the stresses are increased to tensile stress. Therefore, it is proposed the foil thickness cannot exceed 80 μm.

How to design the thickness of foil metal is an important issue. Actually there is not any report on this up to now. Here we compared the maximum principle stress with the yield strength, which is a simplified method. It will be conservative and safe.

4. Conclusions

This study performs a brazed residual stress in BCS design of planar SOFC by three-dimensional finite element method. The effect of the foil thickness on residual stress has been discussed.

(1) The peak residual stresses are shown in the foil and BNi2, and the foil thickness has a great effect on residual stress in BCS structure.
(2) With an increase of foil thickness, the residual stresses are increased in window frame, while they are decreased in Ag–CuO filler metal.
(3) The peak residual stresses in foil and BNi2 filler metal are increased as the foil thickness increases. Too thick foil can lead to large increase of stress in BNi2 and window frame. Based on a compressive consideration, it is proposed that the foil thickness should not exceed 80 μm.

Acknowledgments

The authors gratefully acknowledge the support provided by the National Natural Science Foundation of China (51105380), Doctoral Program of Higher Education of China (20100133120008), Natural Science Foundation of Shandong Province (ZR2010AQ002), Fundamental Research Funds for the Central Universities (10CX04030A) and Key Laboratory of Pressure System and Safety (MOE), East China University of Science and Technology.

References

[1] K. Wang, D. Hissel, M.C. Péra, N. Steiner, D. Marra, M. Sorrentino, C. Pianese, M. Monteverde, P. Cardone, J. Saarinen, Int. J. Hydrogen Energy 36 (12) (2011) 7212–7228.
[2] T. Horita, H. Kshimoto, K. Yamaji, N. Sakai, Y. Xiong, M.E. Brito, H. Yokokawa, Int. J. Hydrogen Energy 33 (14) (2011) 3962–3969.
[3] T.-J. Huang, M.-C. Huang, Int. J. Hydrogen Energy 33 (19) (2008) 5073–5082.
[4] L. Blum, S.M. Groß, J. Malzbender, U. Pabst, M. Peksen, R. Peters, I.C. Vinke, J. Power Sources 196 (17) (2011) 7175–7181.
[5] Y.-S. Chou, E.C. Thomsen, R.T. Williams, J.-P. Choi, N.L. Canfield, J.F. Bonnett, J.W. Stevenson, A. Shyam, E. Lara-Curzio., J. Power Sources 196 (5) (2011) 2709–2716.
[6] J.W. Fergus, J. Power Sources 147 (1–2) (2005) 46–57.
[7] F. Smeacetto, A. Chrysanthou, M. Salvo, Z. Zhang, M. Ferraris, J. Power Sources 190 (2) (2009) 402–407.
[8] K.D. Meinhardt, D.S. Kim, Y.-S. Chou, K.S. Weil, J. Power Sources 182 (1) (2008) 188–196.
[9] C. Story, K. Lu, W.T. Reynolds, D. Brown Jr., Int. J. Hydrogen Energy 33 (14) (2008) 3970–3975.
[10] H. Yoshida, H. Yakabe, K. Ogasawara, T. Sakurai, J. Power Sources 157 (2) (2006) 775–781.
[11] M.C. Tucker, C.P. Jacobson, L.C. De Jonghe, S.J. Visco, J. Power Sources 160 (2) (2006) 1049–1057.
[12] J. Milhans, D.S. Li, M. Khaleel, X. Sun, M.S. Al-Haik, Adrian Harris, H. Garmestani, J. Power Sources 196 (13) (2011) 5599–5603.
[13] S. Le, K. Sun, N. Zhang, M. An, D. Zhou, J. Zhang, D. Li, J. Power Sources 161 (2) (2006) 901–906.
[14] Y.-S. Chou, J.W. Stevenson, J. Power Sources 115 (2) (2003) 274–278.
[15] Y.-S. Chou, J.W. Stevenson, J. Power Sources 124 (2) (2003) 473–478.
[16] K.S. Weil, J.S. Hardy, B.J. Koeppel, J. Mater. Eng. Perform. 15 (4) (2006) 427–432.
[17] K.S. Weil, B.J. Koeppel, Int. J. Hydrogen Energy 33 (14) (2008) 3976–3990.
[18] K. Scott Weil, C.A. Coyle, J.T. Darsell, G.G. Xia, J.S. Hardy, J. Power Sources 152 (1) (2005) 97–104.
[19] S. Le, Z. Shen, X. Zhu, X.L. Zhou, Y. Yan, K. Sun, N. Zhang, Y.X. Yuan, Y. Mao, J. Alloys Compd. 496 (1–2) (2010) 96–99.
[20] M.K. Mahapatra, K. Lu, Mater. Sci. Eng. R: Rep. 67 (5–6) (2010) 65–85.
[21] C. Story, K. Lu, W.T. Reynolds Jr., D. Brown, Int. J. Hydrogen Energy 33 (14) (2008) 3970–3975.
[22] F. Smeacetto, M. Salvo, M. Ferraris, V. Casalegno, P. Asinari, J. Eur. Ceram. Soc. 28 (3) (2008) 611–616.
[23] S. Ghosh, A. Das Sharma, A.K. Mukhopadhyay, P. Kundu, R.N. Basu, Int. J. Hydrogen Energy 35 (1) (2010) 272–283.
[24] T. Zhang, Q. Zhu, Z. Xie, J. Power Sources 188 (1) (2009) 177–183.
[25] H. Apfel, M. Rzepka, H. Tu, U. Stimming, J. Power Sources 154 (2006) 370–378.
[26] S. Le, K. Sun, N. Zhang, Y. Shao, M. An, Q. Fu, X. Zhu, J. Power Sources 168 (2) (2007) 447–452.
[27] Y.-S. Chou, J.W. Stevenson, J. Power Sources 135 (1–2) (2004) 72–78.
[28] J. Duquette, A. Petric, J. Power Sources 137 (1) (2004) 71–75.
[29] Y.-S. Chou, J.W. Stevenson, L.A. Chick, J. Power Sources 112 (1) (2002) 130–136.
[30] H.-T. Chang, C.-K. Lin, C.-K. Liu, J. Power Sources 189 (2) (2009) 1093–1099.
[31] T.L. Jiang, M.-H. Chen, Int. J. Hydrogen Energy 34 (19) (2009) 8223–8234.
[32] W. Fischer, J. Malzbender, G. Blass, R.W. Steinbrech, J. Power Sources 150 (2005) 73–77.
[33] K. Fujita, T. Somekawa, T. Hatae, Y. Matsuzaki, J. Power Sources 196 (2) (2011) 9022–9026.
[34] A. Nakajo, Z. Wuillemin, J. Van Herle, D. Favrat, J. Power Sources 193 (1) (2009) 203–215.
[35] C.-K. Lin, L.-H. Huang, L.-K. Chiang, Y.-P. Chyou, J. Power Sources 192 (2) (2009) 515–524.
[36] K.S. Weil, B.J. Koeppel, J. Power Sources 180 (1) (2008) 343–353.
[37] W. Jiang, S.T. Tu, G.C. Li, J.M. Gong, J. Power Sources 195 (11) (2010) 3513–3522.
[38] W. Jiang, J. Gong, S.-T. Tu, Mater. Des. 31 (1) (2010) 648–653.